The microstructure and biogeochemistry of Arctic cryoconite granules

Harry LANGFORD,[1,2] Andy HODSON,[1] Steve BANWART,[2] Carl BØGGILD[3]

[1]*Department of Geography, University of Sheffield, Winter Street, Sheffield S10 2TN, UK*
E-mail: h.langford@shef.ac.uk
[2]*Kroto Research Institute, University of Sheffield, Broad Lane, Sheffield S3 7HQ, UK*
[3]*The University Centre in Svalbard (UNIS), PO Box 156, NO-9171 Longyearbyen, Norway*

ABSTRACT. A cryoconite granule is a biologically active aggregation of microorganisms, mineral particles and organic matter found on glacier surfaces, often within shallow pools or cryoconite holes. Observations of the microstructure of a range of cryoconite granules from locations in Svalbard and Greenland reveal their structure and composition. Whereas bulk analyses show that the mineralogy and geochemistry of these granules are broadly similar, analyses of their microstructure, using optical, epifluorescence and confocal microscopy, indicate differences in the location and quantity of photosynthetic microorganisms, heterotrophic bacteria and organic matter. Using these findings, a hypothesis on the aggregation of cryoconite is presented, centred upon multilevel aggregation by bioflocculation and filamentous binding.

INTRODUCTION

Recent studies have revealed a fascinating range of glacier ice ecosystems, with high biodiversity considering the extreme environments in which they form (Hodson and others, 2008). The microbial food web is both complex and variable, comprising a variety of autotrophic and heterotrophic microorganisms, fungi and eukaryotic microfauna (Margesin and others, 2002; Hodson and others, 2008). Cryoconite, meaning 'cold dust', is granular organic-rich debris found supraglacially, particularly within 'cryoconite holes', small depressions within the ice. The existence of these holes has been known since the 19th century (von Drygalski, 1897), but only recently have advancements in analytical techniques allowed us to begin to understand the communities of microorganisms living within them and the interaction between these and inputs into the ecosystem, such as sunlight and inorganic nutrients.

Biogeochemical interactions on the surface of the glacier play a key role in entraining and retaining aeolian particulate matter on glaciers, thereby enhancing melt. However, the specific process by which cryoconite aggregates form and sustain themselves has received little research attention. Hodson and others (2010) suggest that both processes are likely to be strongly linked to carbon balance. Further, given the net ablation of many Svalbard glaciers, the aggregation and evolution of cryoconite aggregates and their impact on soil development in recently deglaciated forefield areas need to be given attention. For example, Sigler and Zeyer (2002) find that forefield successional gradients contain a diverse microbial assemblage, increasing in both biomass and activity with age, yet they note that the source(s) of this community and the importance of specific pioneer bacteria are still unclear.

Although the impact of cryoconite has been studied in relation to supraglacial biogeochemistry (e.g. Hodson and others, 2008; Stibal and others, 2008), and the microbiology of cryoconite is now well characterized in various environments (e.g. Margesin and others, 2002; Christner and others, 2003), specific studies on the microstructure and biogeochemistry of cryoconite are few (Takeuchi and others,

2001a,b). As noted by Dittrich and Luttge (2008), there is increasing evidence that microorganisms obtain competitive advantage through using their reactive cell surfaces as interfaces to actively control water–solid interactions. Microscopic imaging is becoming an increasingly important tool for investigating hydrated, biologically active structures, due to its being non-invasive, three-dimensional (3-D) and having the ability to cover many spatial scales (Neu and others, 2010). In recent years, a range of microscopic imaging methods have been employed, with confocal laser scanning microscopy (CLSM) leading the way. Using specific fluorescent probes, the structure, composition and microhabitats of biological samples have now been investigated (Chen and others, 2007; Neu and others, 2010). For example, CLSM has quantified the spatial distribution and structural form of extracellular polymeric substances (EPS): glue-like substances vital for the formation of aggregates and composed of microbial polysaccharides, proteins, nucleic acids and polymeric lipophilic compounds (e.g. Lawrence and others, 2003). To hypothesize on the aggregation and development of cryoconite, it is necessary to gain a comprehensive understanding of its microstructure and the variation of this microstructure across differing biogeochemical environments. A novel combination of microscopic and spectroscopic techniques is therefore used below to better understand the microstructure and biogeochemistry of cryoconite granules from three glaciers in Svalbard: Vestfonna (VF) in western Nordaustlandet, Midtre Lovénbreen (ML) in the Kongsfjord region of western Spitsbergen, and Longyearbreen (LY) in the Isfjord region of western Spitsbergen; and two areas on the Greenland ice sheet: Kronprins Christian Land (KP) in northeast Greenland, and Kangerlussuaq (KG) in southwest Greenland.

METHODOLOGY

All cryoconite was sampled in the field using sterile implements and sterile containers, and was transferred frozen and stored at –20°C until just prior to analysis. To enable microstructural analyses to be undertaken, a range of

thin-section techniques were developed, as outlined below. These techniques reduced problems associated with the attenuation of light intensity (Barranguet and others, 2004). This cross-sectional approach, combined with bulk and surface analyses, therefore enabled the structure and composition of cryoconite granules to be studied in great detail. The methodological approach can be split into mineralogical and geochemical analyses, performed principally on dried cryoconite, and microbiological and biochemical analyses, performed principally on defrosted, hydrated cryoconite.

Mineralogical and geochemical analyses

Ten cryoconite granules were dried at low temperature (35°C), infiltrated with an Araldite resin under vacuum, ground and polished until a thin section of ~30 μm thickness was produced. These thin sections were analysed using a bright-field, cross-polarizing microscope with single-lens reflex (SLR) camera attachment. To complement the mineralogical characterization undertaken on thin sections, bulk mineralogical investigations using powder X-ray diffraction (XRD) and KBr-pellet Fourier transform infrared (FTIR) spectroscopy were employed. Powder XRD was performed on a Siemens D500 powder diffractometer (Cu-source), with 150 mg of finely powdered cryoconite, at angles of 5–70°, at $1°\,min^{-1}$ and with a step size of 0.02. KBr FTIR was performed on a Perkin-Elmer Spectrum One, with 3 mg of finely ground cryoconite and 150 mg of KBr granules (1 : 50 ratio), pressed into a disc under 10 N force in a die press; 100 scans were sequentially recorded and averaged. The absorbance of KBr was accounted for by running blanks consisting of solely KBr powder.

Granule size, constituent-particle size and organic-matter analyses were also undertaken on dried cryoconite subsamples. Granule size analyses were performed in order to assess the morphology of the whole cryoconite granules and its variability. An 'imaging chamber' was constructed by cutting a well into cellophane tape that had been layered on a glass slide. Five hundred milligrams of cryoconite granules from each location were deposited into the well and imaged using a dissecting microscope with charge-coupled device (CCD) camera attachment (bright-field reflected light and 1× magnification). The raw images were subsequently adjusted for brightness and contrast, and, using ImagePro Plus (Media Cybernetics, Silver Springs, USA), the 'area' function was used to calculate the projected two-dimensional area of the granules; any touching granules were manually separated. The average diameter of each granule was calculated using the formula (length + width)/2.

Particle size analyses of constituent particles followed disaggregation by boiling the aggregates in a 30% hydrogen peroxide solution for 1 hour and until effervescence ceased. Analysis was then undertaken in triplicate (following standard operating protocols) on a Horiba LA950 laser diffraction particle sizer.

Bulk organic matter content and composition were determined using step-wise thermogravimetric analysis, based on the protocol of Kristensen (1990). Five hundred milligrams of each sample was heated in a muffle furnace at 105°C, 200°C, 350°C and 520°C, for 4 hours at each temperature, allowed to cool within a desiccator and weighed. This procedure enables the calculation of total organic carbon (TOC) contents, as well as the differentiation of thermo-labile (200–350°C) and thermo-stable organic matter (350–520°C) (Cuypers and others, 2002).

Microbiological and biochemical analyses

Fully hydrated cryoconite granules were dropped into a small amount of ultrahigh-quality (UHQ) water and immediately frozen using liquid nitrogen. These blocks of cryoconite and amorphous ice were then sectioned at –15°C within a cryostat, to a thickness of 60 μm, and deposited on a Superfrost™ glass microscope slide. Sections were allowed to dry for 1 hour at room temperature and were then stained with various fluorescent biological stains.

The development of a multiple fluorescent staining protocol to stain thin sections of cryoconite material and image using CLSM requires the consideration of autofluorescence, particularly from photosynthetic microorganisms, which can directly interfere with the fluorochromes used (Neu and others, 2002). Consequently, a three-pronged approach was employed, using 4',6-diamidino-5-phenylindole (DAPI) to stain cellular material, AlexaFluor 488 (concanavalin A conjugate) to stain the polysaccharides within EPS, and autofluorescent emission to visualize photosynthetic microorganisms. This approach was developed based on the protocols of Neu and others (2004) and Chen and others (2007). The autofluorescence of photosynthetic microorganisms was excited at 543 nm and detected between 650 and 700 nm. Each thin section was therefore covered with 100 μL of DAPI stain (12.5 μg mL^{-1} final concentration) and incubated for 5 min in the dark. This stain solution was then removed by pipette, and the thin section was washed with a 100 μL drop of UHQ water, three times for 5 min durations. Following this, a 100 μL drop of AlexaFluor 488 (concanavalin A conjugate) fluorescent dye was added (at 100 μg mL^{-1} final concentration), incubated for 20 min in the dark and then washed as described above. Each thin section was subsequently imaged on a Zeiss LSM 510 META microscope with two-photon capabilities.

To characterize the bulk microbial biomass of cryoconite debris, a small amount (10 mg) of thawed cryoconite was resuspended in 1 mL of UHQ water, buffered with phosphate-buffered saline (PBS), and incubated with DAPI stain as described above, filtered onto a 0.2 μm black polycarbonate filter paper and mounted onto a glass slide. These slides were analysed and imaged under fluorescent light using a Zeiss Axioplan 2 epifluorescence microscope with a DAPI filter cube. Autofluorescence of both photosynthesizing microorganisms and certain inorganic particulates was detected using the FITC broad filter. Due to the attachment of biota to mineral surfaces, a z-section technique was employed, whereby 15 random fields of view were imaged at 0.5 μm z-intervals and cell counts undertaken on these images.

RESULTS

Geological and geochemical

Figure 1 illustrates some of the typical spectral profiles obtained using powder XRD and KBr FTIR. XRD analyses indicate a prevalence of silicate minerals and their weathering products (Cullity, 1978; Ruffell and Wiltshire, 2004). The strongest peaks correspond well to the International Centre for Diffraction Data (ICDD) file 46-1045, indicating an abundance of quartz. Cryoconite from KP shows the simplest diffraction pattern, indicative of a mineralogy dominated by quartz, with contributions from orthoclase and plagioclase feldspar. Cryoconites from VF and ML show similar diffraction patterns, with data suggesting a dominance by quartz,
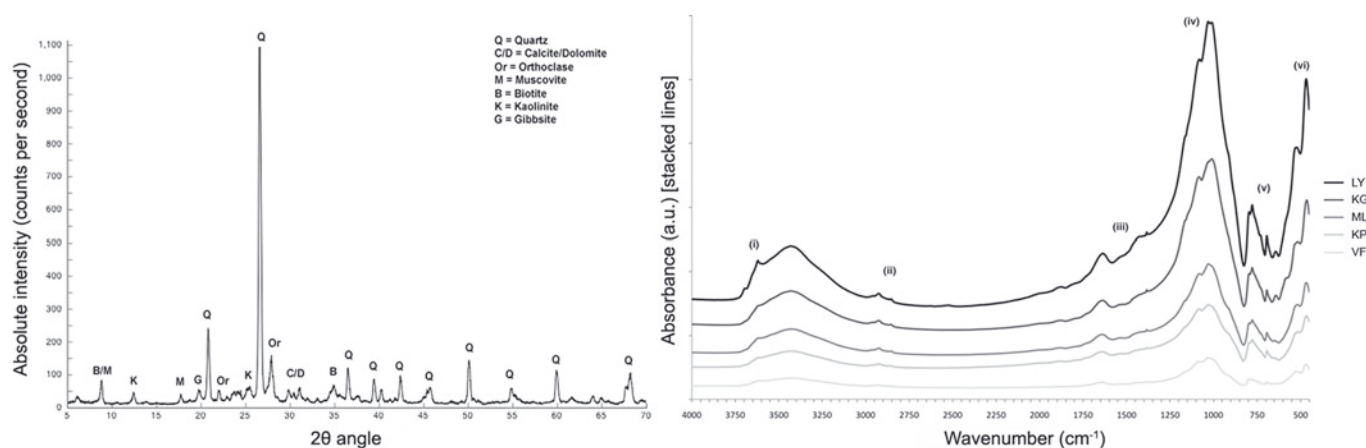
Fig. 1. Mean combined powder XRD profile, an example to illustrate interpretation, showing the dominance of silicate minerals and their weathering products. Typical KBr FTIR profiles for each of the cryoconite samples; features of interest (i–vi) are discussed in the text.

with significant contributions by mica, kaolinite-type clays, and orthoclase feldspar. Silicates and dolomite dominate the diffraction pattern from LY, as outlined by Hodson and others (2010). Cryoconite from KG shows the most complex signal, suggesting a broader mineralogy with a greater dominance by plagioclase feldspar, and contributions from calcareous minerals and apatite. FTIR spectra complement the XRD data, in that the peak assignments indicate a prevalence of quartz and weathered silicates. The peaks at $\sim$3430 cm^{-1} and $\sim$1640 cm^{-1} can be attributed to 'free' water within the sample. The labelled groups of peaks can be attributed as follows: (i) stretching of inner hydroxyl groups between tetrahedral and octahedral sheets of phyllosilicates (e.g. kaolinite, illite and smectite), (ii) aliphatic C–H stretching indicative of organic acids and lipids, (iii) calcite and dolomite peaks at $\sim$1430 cm^{-1} and $\sim$1450 cm^{-1} respectively, (iv) Si–O stretching vibrations of phyllosilicates, (v) vibrations that can be largely attributed to quartz, and (vi) Si–O–metal bending bands (Madejová, 2003; Madejová and others, 2009). When the phyllosilicate vibrations are studied in more detail, it is clear that all cryoconite samples show a peak at $\sim$1026–1034 cm^{-1}, indicative of biotite, illite and kaolinite (A. Matteson and M.A. Herron, http://www.scaweb.org/assets/papers/1993_papers/1-SCA1993-08.pdf). Most cryoconite samples also show a shoulder at $\sim$1016–1000 cm^{-1}, indicative of muscovite and orthoclase feldspar, with KG cryoconite showing a pronounced peak at 1004 cm^{-1}, indicative of glauconite (Matteson and Herron, 1993).

Optical microscopy of geological thin sections revealed that mineral particles were typically <100 µm in diameter and showed evidence of weathering and organic coatings. The organo-mineral groundmass showed evidence of zoning and clustering, and varying degrees of humification. In agreement with the XRD and FTIR data, it was also found that the three principal mineralogies were quartz, orthoclase feldspar and micas, with calcite, clays, trace minerals and organic matter making up a varying proportion of the remaining solid material. For example, KP cryoconite in Figure 2 shows an abundance of quartz, low quantities of mica and feldspar, and small regions of organic material (i), some organic coatings on particles and a rich organic layer around one edge (ii). ML cryoconite in Figure 2 shows a heterogeneous distribution of quartz, orthoclase feldspar and mica, with a higher and more variable quantity of clay-sized particles, with larger quantities and regions of organic

matter (iii), as well as a dark, organic layer near the edge of the granule (ii). Differences in granule composition were evident between granules from the same sampling location, especially from KP, where thin sections revealed a continuum between aggregations of minerals with near-transparent organic matter between the mineral particles, and rarer aggregations of minerals surrounded by near-opaque green to black organic matter. The opacity and colour of organic matter within the granule may well be directly influenced by the age of the aggregate, though other factors such as the accumulation of microbial pigments or colloidal black carbon particles may also be significant.

Cryoconite particle size analyses found that silt was the dominant particle size (following Gale and Hoare, 1991) at four of the five sampling locations. Cryoconites from KG and VF were found to have the highest clay contents (<3 µm), cryoconite from ML showed the highest sand content (>63 µm), and cryoconites from KP and VF showed the highest silt contents (3–63 µm). The median and mean particle sizes varied from 64.754 and 80.492 µm at ML, to 16.315 and 28.830 µm at VF, respectively. It must be noted, however, that the majority of particle size data were non-normal in form.

Comparing the aggregate size distribution, cryoconites from KG and KP showed the smallest mean aggregate sizes ($\sim$400 µm), while ML and LY showed mean aggregate sizes of $\sim$500 µm, and cryoconite from VF showed the highest mean aggregate size ($\sim$600 µm). A more comprehensive study of aggregate size on LY using field-based imagery (Hodson and others, 2010) found a considerably larger aggregate size (median 6.74 mm), perhaps indicating that in situ, hydrated aggregates are significantly larger.

Triplicate thermogravimetric analyses found that organic matter content (as a percentage of dry weight) varied from 1.30% for cryoconite from KG, to 6.07% for VF. Cryoconite from KP, LY and ML exhibited TOC values of 1.48%, 2.76% and 3.27% respectively. These are in agreement with TOC values determined for cryoconite from other Svalbard glaciers (e.g. Štibal and others, 2008). The Rp values (Kristensen, 1990) for Arctic cryoconite, a ratio of mass loss between 200°C and 350°C and mass loss between 350°C and 520°C, were all <0.5, indicating that the majority of organic matter present within these aggregates is thermolabile, i.e. dominated by carbohydrates (Kristensen, 1990; Siewert, 2004).
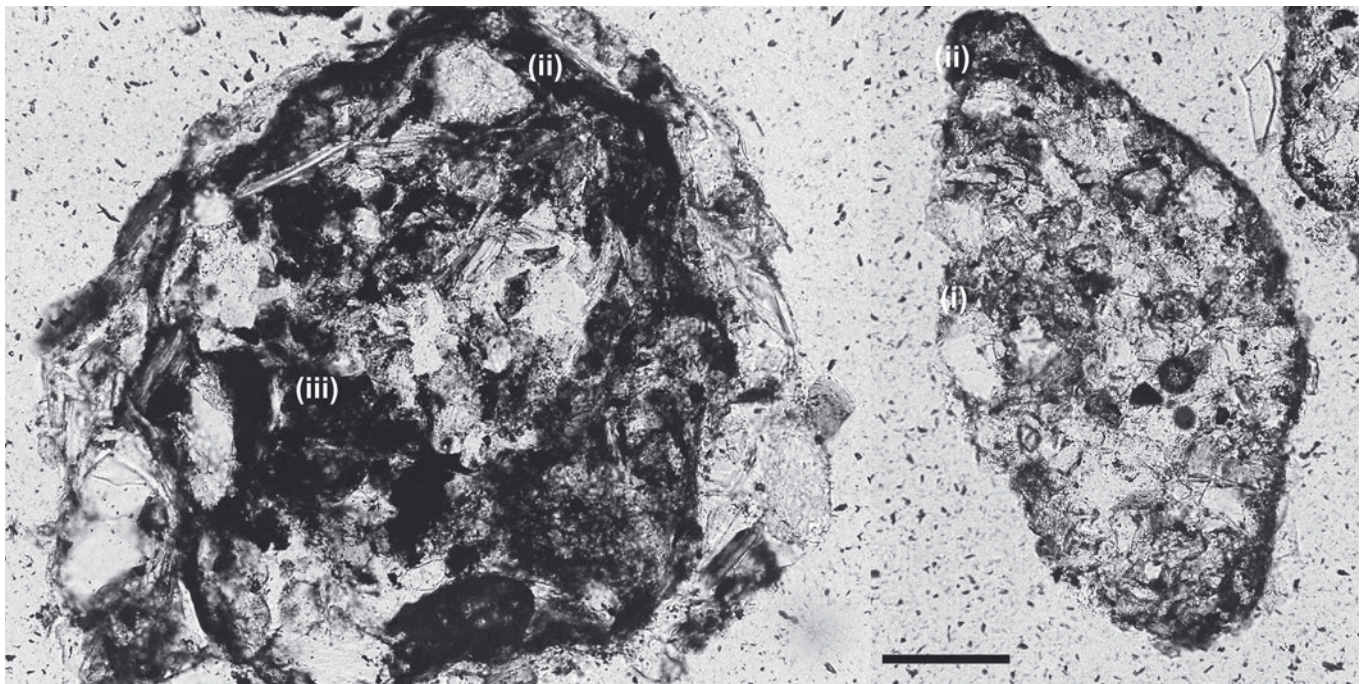
Fig. 2. Low-magnification (20×) bright-field imagery of, from left, ML cryoconite granule and KP cryoconite granule. Zoning of mineral grains and organic matter is evident, with translucent green-yellow organic matter clustering near the granule edge (i), and opaque near-black organic matter evident both as a layer around/near the granule edge (ii) and as clustering within the centre of an organic-rich granule (iii); scale bar is 100 µm.

Biological and biochemical

Total counts of DAPI-stained cryoconite indicated between $\sim1.95 \times 10^3$ cells mg^{-1} for KG cryoconite and 1.05×10^4 cells mg^{-1} for VF cryoconite. Cryoconite from KP showed a similar total count to VF (9.07×10^3 cells mg^{-1}), with LY and ML cryoconite showing 2.18×10^3 and 2.57×10^3 cells mg^{-1} respectively. The majority of DAPI-stained microorganisms were found to be either coccoid in shape or filamentous, with some rod and a few vibrio also present. Autofluorescence imagery indicated the presence of variable quantities and types of photosynthetic microorganisms. Microscopic analysis has identified, based on the classification system of Rippka and others (1979), a dominance of filamentous cyanobacteria, particularly thinner *Leptolyngbya* sp. (diameter 0.7–2 µm), and thicker *Phormidium* sp., *Lyngbya* sp. and *Oscillatoria* sp. (diameter 4–11 µm). Unicellular cyanobacteria, probably *Synechococcus* sp. or *Gloeocapsa* sp., various algae and diatoms have also been identified.

Low-magnification CLSM images (Fig. 3a–d) indicated the heterogeneous distribution of photoautotrophs within cryoconite. KG cryoconite (image not shown) contained a relatively low microbial content. KP cryoconite showed a dominance of heterotrophic bacteria and infrequent clusters of unicellular photoautotrophs (Fig. 3a), whereas ML and LY cryoconite (Fig. 3b and c respectively) showed a greater prevalence of photoautotrophs and clusters of heterotrophic bacteria, and VF cryoconite (Fig. 3d) aggregates showed the highest prevalence of photosynthetic microorganisms, as well as a prevalence of heterotrophic bacteria. While it is appreciated that chemoautotrophic bacteria and archaea may also be present, the differentiation of photoautotrophs and heterotrophs using autofluorescence and nuclear staining has been the traditional approach when studying phototrophic biofilms (e.g. Neu and others, 2004). ML and LY aggregates supported a greater number of thicker

filaments *(Phormidium* sp. and *Oscillatoria* sp.), whereas VF aggregates seemed to principally contain a far denser network of thinner filaments (Leptolyngbya sp.). Unicellular photosynthetic microorganisms were rarely seen to dominate, and were often found associated with clusters of filamentous microorganisms. Larger single-celled photo-trophs, likely green algae, were found sporadically throughout the granule, either singly or as small colonies. As evidenced in Figure 3d, aggregates enriched with filamentous cyanobacteria tended to exhibit a denser network of filaments at or just below the surface, in this case extending for $\sim$50–70 µm into the granule and providing structural support for the aggregate. Aggregates impoverished in filamentous cyanobacteria (Fig. 3a) showed disruption when cut with a microtome blade, indicative of a more fragile aggregate structure. Within cryoconite aggregates, filament orientation was generally random and encapsulated mineral particles. Aggregates with a dense network near the surface showed a slightly greater tendency for filaments to orient parallel to the surface of the granule, perhaps to maximize the surface area exposed to sunlight. Figure 3a–d also illustrate that polysaccharides could be found covering the surfaces of mineral particles, with greater concentrations of polysaccharides nearly always associated with clusters of photoautotrophs. Furthermore, high concentrations of polysaccharides were most evident at or near the surface of cryoconite granules (Fig. 3d). Those aggregates showing a relatively homogeneous distribution of polysaccharides throughout, such as those from LY (Fig. 3c), showed a finer fabric, suggestive of strong clay–organic-matter interactions.

Figure 3e indicates two separate autofluorescent emissions captured using short pass filters covering the wavelength ranges 650–700 nm (pink) and 590–650 nm (yellow), in this case for a biofilm mechanically removed from the surface of a cryoconite granule from ML. It can be seen that
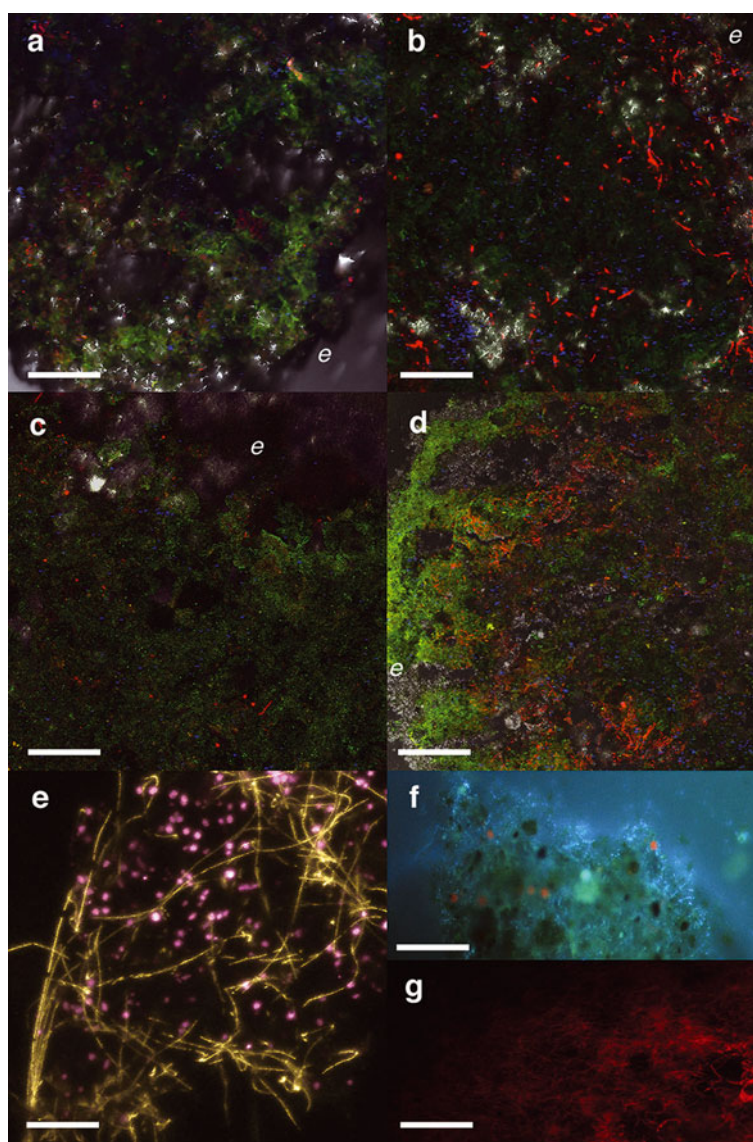
Fig. 3. CLSM images showing (a–d) variation in photoautotrophic microorganism (red; autofluorescence), heterotrophic microorganism (blue; DAPI) and polysaccharide contents (green; AlexaFluor 488) of cryoconite aggregates (*e* is outer edge of aggregate); (e) differentiation of photosynthetic pigments using their fluorescent emissions; (f, g) epifluorescent images detailing a heterotroph-rich and an autotrophic filament-rich granule respectively; scale bars are 50 µm.

the stronger fluorescent emissions (coloured pink) emanated from the unicellular microorganisms. In fact, emission spectra for these unicellular microorganisms, taken from lambda stack images using a 'region of interest' filter, showed a fluorescence peak at ~678 nm, which can be correlated with chlorophyll *a* content (Barranguet and others, 2004). The slightly weaker fluorescent emissions (coloured yellow) emanated from the filamentous microorganisms, with emission spectra indicating a fluorescence peak at ~645 nm, which can be correlated with phycocyanin, a cyanobacterial phycobiliprotein.

Both CLSM- and epifluorescence-based analyses of heterotrophic bacteria confirmed their heterogeneous occurrence throughout cryoconite aggregates. The low-magnification CLSM images in Figure 3 indicate that they tend to cluster in greatest numbers in areas often associated with photoautotrophic activity and the presence of organic matter. In cryoconite from KP, greater concentrations of heterotrophic bacteria were found at the edge of the granule, clearly visualized in Figure 3f. This is in direct contrast to the filament-rich surface layer dominating in cryoconite from VF (Fig. 3g), for example.

DISCUSSION

Microstructure and biogeochemistry of Arctic cryoconite

In summary, optical microscopy, XRD and KBr FTIR analyses found that Arctic cryoconite granules are dominated by phyllosilicate, tectosilicate and quartz minerals, showing a dominance of small particle sizes (<100 µm) and a varying but significant quantity of organic groundmass, characterized by varying degrees of pigmentation and/or humification. Mineral coatings are also prevalent, with constituent mineral particles showing both organic and metal oxide/hydroxide coatings. These findings are in agreement with other biogeochemical and structural investigations of cryoconite from the Arctic and elsewhere in the world (Takeuchi and others, 2001a,b; Štibal and others, 2008;

Hodson and others, 2010). Clear differences in the mineralogy and geochemical aggregate structure can be seen both when comparing cryoconite from different glaciers and when comparing cryoconite from one sampling location on a single glacier. This structural heterogeneity allows for the existence of microenvironments exhibiting different physicochemical and structural characteristics (Ranjard and Richaume, 2001); indeed Carson and others (2009) find that mineral heterogeneity directly contributes to the spatial variation in bacterial communities. Fine-textured sediment can be seen to promote microbial abundance, in accord with Štibal and others (2006). In addition, the data indicate a relationship between mean organic matter content and mean aggregate size, most clearly seen when comparing cryoconite granules from VF and KP. This relationship can also be seen in soil micro-aggregates, whereby the interaction of microbial biomass within the soil, governed by variations in the microbiology and soil properties (particularly texture, clay mineralogy, pore-size distribution and aggregate dynamics), can culminate in the protection of microbially produced organic matter through aggregation (Six and others, 2006). Arctic cryoconite has been shown by thermogravimetry to be dominated by thermolabile carbohydrates, suggesting that microbial EPS contributes significantly to the stabilization of these aggregates, both through its own cohesive properties and by moderating the surface chemistry of nearby substrates, promoting cation exchange and interaction with fine clay and colloid fractions (Kögel-Knabner and others, 2008).

Fluorescence microscopy techniques indicated that cryoconite granules are rich in microorganisms, with total counts comparing favourably with recent literature (Štibal and others, 2008). CLSM images illustrated a heterogeneous distribution throughout the granule and evidence of clustering and association with organic matter. In agreement with Takeuchi and others (2001a,b) and Hodson and others (2010), the majority of aggregates of organic-rich cryoconite, such as upon VF, showed a network of filamentous cyanobacteria on or near the surface. Cyanobacterial filaments showed a broad range of morphotypes, as evidenced in other glacial environments (de los Ríos and others, 2004). This network did not appear to show a dominant orientation, but does entangle mineral particles and support clusters of unicellular photoautotrophs, heterotrophic bacteria, and a prevalence of organic matter within its surround. Not all cryoconite can be said to conform to the above description, however, as cryoconite from KP in particular shows a greater concentration of filamentous and unicellular heterotrophic bacteria, dominating the near surface of the granule, and a sporadic distribution of photoautotrophs, chiefly unicellular cyanobacteria and algae. In contrast to aggregates from VF, which show little change in size upon light agitation, aggregates from KP disaggregate into smaller micro-aggregates (or flocs). These are generally composed of a cluster of heterotrophic bacteria surrounding an aggregation of organic matter, with some small mineral particles entrained and occasionally a single cyanobacterial filament. Indeed these micro-aggregates show a similarity to 'marine snow': suspended aggregates rich in microbia, organic matter and trace metals (Simon and others, 2002). Furthermore, fluorescent images of cryoconite aggregates indicate that, in general, there is a positive relationship between the number of photoautotrophic microorganisms and aggregate size. This is likely to be due to filamentous binding and the presence of cyanobacterial EPS. It has been shown that cyanobacterial filaments actively form ligand–metal complexes (Yee and others, 2004) and, as such, can interact and readily bind with clays and organic matter. A long summer without disruption by snowfall has been identified as a key factor in the proliferation of cyanobacteria and algae on the glacier surface (Yoshimura and others, 1997).

EPS plays an important role in the microstructure of aggregates from other environments, since it can assist cell–cell attachment by forming bridging complexes, alter the surface charge of dispersed cells or filaments, allowing coagulation, and also provide protection from abiotic stress and predation (Schmidt and Ahring, 1994; Adav and others, 2010). Further, the trapping of particulate matter and adsorption of nutrients by EPS in aquatic environments enables functional advantages, such as assisting in the formation of sedimentable aggregates and providing diverse microenvironments for nutrient uptake (Leppard, 1995). Zulpa de Caire and others (1997) found that aggregate size and stability both increase when either EPS or cyanobacteria are inoculated into soil, with solely EPS showing only a short-term aggregating influence, as opposed to cyanobacteria, which show a long-term influence. It has been proposed (de Winder and others, 1999) that the exopolymer sheaths of cyanobacteria are, to an extent, recalcitrant to mineralization, and as such their cohesive binding effect on sediment can be maintained. Consequently, it may be said that microbial composition can fundamentally affect the microstructure and composition of cryoconite granules. A continuum is evident, between cryoconite aggregates that are dark, dense structures compiled of a large number of cyanobacterial filaments, and cryoconite aggregates that are lighter, gelatinous structures compiled of smaller micro-aggregates showing greater dominance by heterotrophic microorganisms. While one end-member is more akin to microbial mats and soil micro-aggregates, the other is more akin to sludge flocs and marine snow.

Implications for cryoconite aggregate formation

The data reported above, as well as current knowledge within the literature, allow a hypothesis for cryoconite aggregation to be developed. Given the prevalence of photosynthetic microorganisms within cryoconite, it is clear that they are actively involved in the aggregation of cryoconite granules. As such, it is proposed that:

1. Photosynthetic blooms in near-surface suspension (witnessed at sites across Svalbard; personal communication from A. Hodson, 2010) result in micro-aggregations of EPS and both filamentous and unicellular photoautotrophs in wet snow and slush. Here aeolian colloidal particulates also aggregate through physico-chemical interaction, such as hydrophobic interaction of black carbon and perikinetic and orthokinetic flocculation (Folkersma and others, 1999), while interactions between planktonic bacteria and clay-sized particles result in biofilm development (Zavarzin and Alekseeva, 2009). These are all potential precursory steps that could take place on glaciers, with the 'straining' of particulates from meltwaters percolating through snow physically promoting interaction.

2. EPS-rich micro-aggregates will grow further by acting as sticky sieves that trap suspended or settling particulates

in transit across the glacier. EPS provides an extensive surface area for binding, with total concentrations of electrostatic binding sites being >20 times higher than for cell surfaces (Liu and Fang, 2002), as well as containing both hydrophobic and hydrophilic polymers (Jorand and others, 1998) and having the ability to partially overcome a cell's negative charge (Tsuneda and others, 2003).

3. Increasing aggregation leads to a greater settling ability and, due to dark particulate matter within these micro-aggregates, differential melt into the ice (Wharton and others, 1985). As with other bio-aggregates, it is likely that filamentous binding then takes over as the dominant influence on aggregate structure and development. Given the CLSM observations discussed above, it is considered that certain aggregates and locations do not support a proliferation of cyanobacterial filaments. These aggregates, as in KG for example, are therefore weakly bound with sporadic cyanobacterial filaments, meaning that they can be disrupted by increases in shear strength. In aggregates and locations where the biogeochemistry is conducive to cyanobacterial proliferation, such as in VF, filaments do indeed proliferate, mechanically and chemically binding the aggregate substrate. Cyanobacteria, being slow-growing, should positively influence the density and stability of bio-aggregates (de Kreuk and Van Loosdrecht, 2004).

4. The fate of cryoconite aggregates after the above growth stages is most likely dominated by stochastic transport events that result from glacier ablation during the summer. On gentle sloping ice surfaces, the persistence of cryoconite for several years appears possible (Hodson and others, 2010), while those aggregates that combine to form cryoconite holes in close proximity to migrating supraglacial streams are at greater risk of transfer from the system (Takeuchi and others, 2000).

CONCLUSIONS

It is clear that the cryoconite granule is a complex, heterogeneous entity showing broad similarities in structure and composition across the Arctic region, yet showing variability even between granules within the same cryoconite hole. The dominance of filamentous microorganisms within the strongest granules, particularly cyanobacteria, points towards the pivotal role these bacteria play in the stable aggregation of supraglacial sediments. However, the roles of other photosynthetic microorganisms and heterotrophic bacteria are clearly elevated in some granules. When combined with the fact that polysaccharides were present in all granules studied, this suggests that EPS also has an important role to play in the aggregation of cryoconite. The tight clustering of organic matter, photo-trophs and heterotrophs in many granules suggests a relationship between autotrophy and heterotrophy within cryoconite, with implications for carbon cycling within aggregates. Furthermore, it is clear that various geochemical factors can support aggregation, in particular the availability of weathered minerals and colloidal particles. A theory of cryoconite aggregate formation has been hypothesized, centred upon multilevel aggregation, with bioflocculation and filamentous bulking the two key steps. Knowledge of the roles of photosynthetic microorganisms and EPS in aggregation is still, however, in its infancy, and it

is thought vital to further this research in order to better understand supraglacial ecosystems.

REFERENCES

Adav, S.S. *and 6 others*. 2010. Stereological assessment of extracellular polymeric substances, exo-enzymes, and specific bacterial strains in bioaggregates using fluorescence experiments. *Biotech. Adv.*, **28**(2), 255–280.

Barranguet, C. *and 6 others*. 2004. Studying undisturbed auto-trophic biofilms: still a technical challenge. *Aquat. Microbial Ecol.*, **34**(1), 1–9.

Carson, J.K., L. Campbell, D. Rooney, N. Clipson and D.B. Gleeson. 2009. Minerals in soil select distinct bacterial communities in their microhabitats. *FEMS Microbiol. Ecol.*, **67**(3), 381–388.

Chen, M.-Y., D.-J. Lee, J.-H. Tay and K.-Y. Show. 2007. Staining of extracellular polymeric substances and cells in bioaggregates. *Appl. Microbiol. Biotech.*, **75**(2), 467–474.

Christner, B.C., B.H. Kvito and J.N. Reeve. 2003. Molecular identification of bacteria and eukarya inhabiting an Antarctic cryoconite hole. *Extremophiles*, **7**(3), 177–183.

Cullity, B.D. 1978. *Elements of x-ray diffraction. Second edition.* Reading, MA, Addison-Wesley.

Cuypers, C., T. Grotenhuis, K.G.J. Nierop, E.M. Franco, A. de Jager and W. Rulkens. 2002. Amorphous and condensed organic matter domains: the effect of persulfate oxidation on the composition of soil/sediment organic matter. *Chemosphere*, **48**(9), 919–931.

De Kreuk, M.K. and M.C.M. van Loosdrecht. 2004. Selection of slow growing organisms as a means for improving aerobic granular sludge stability. *Water Sci. Technol.*, **49**(11–12), 9–17.

De los Ríos, A., C. Ascaso, J. Wierzchos, E. Fernández-Valiente and A. Quesada. 2004. Microstructural characterization of cyano-bacterial mats from the McMurdo Ice Shelf, Antarctica. *Appl. Environ. Microbiol.*, **70**(1), 569–580.

De Winder, B., N. Staats, L.J. Stal and D.M. Paterson. 1999. Carbohydrate secretion by phototrophic communities in tidal sediments. *J. Sea Res.*, **42**(2), 131–146.

Dittrich, M. and A. Luttge. 2008. Microorganisms, mineral surfaces, and aquatic environments: learning from the past for future progress. *Geobiology*, **6**(3), 201–213.

Folkersma, R., A.J.G. van Diemen and H.N. Stein. 1999. Under-standing the influence of gravity on perikinetic coagulation on the basis of the DLVO theory. *Adv. Colloid Interface Sci.*, **83**(1–3), 71–84.

Gale, S.J. and P.J. Hoare. 1991. *Quaternary sediments.* London, Belhaven Press.

Hodson, A. *and 7 others*. 2008. Glacial ecosystems. *Ecol. Monogr.*, **78**(1), 41–67.

Hodson, A. *and 6 others*. 2010. The structure, biological activity and biogeochemistry of cryoconite aggregates upon an Arctic valley glacier: Longyearbreen, Svalbard. *J. Glaciol.*, **56**(196), 349–362.

Jorand, F., F. Boue-Bigne, J.C. Block and V. Urbain. 1998. Hydrophobic/hydrophilic properties of activated sludge exo-polymeric substances. *Water Sci. Tech.*, **37**(4), 307–315.

Kögel-Knabner, I. *and 7 others*. 2008. Organo-mineral associations in temperate soils: integrating biology, mineralogy, and organic matter chemistry. *J. Plant Nutr. Soil Sci.*, **171**(1), 61–82.

Kristensen, E. 1990. Characterization of biogenic organic matter by stepwise thermogravimetry. *Biogeochemistry*, **9**(2), 135–159.

Lawrence, J.R. *and 6 others*. 2003. Scanning transmission X-ray, laser scanning, and transmission electron microscopy mapping of the exopolymeric matrix of microbial biofilms. *Appl. Environ. Microbiol.*, **69**(9), 5543–5554.

Leppard, G.G. 1995. The characterization of algal and microbial mucilages and their aggregates in aquatic ecosystems. *Sci. Total Environ.*, **165**(1–3), 103–131.

Liu, H. and H.H.P. Fang. 2002. Characterization of electrostatic binding sites of extracellular polymers by linear programming analysis of titration data. *Biotech. Bioeng.*, **80**(7), 806–811.

Madejová, J. 2003. FTIR techniques in clay mineral studies. *Vibr. Spectrosc.*, **31**(1), 1–10.

Madejová, J., M. Pentrák, H. Pálková and P. Komadel. 2009. Near-infrared spectroscopy: a powerful tool in studies of acid-treated clay minerals. *Vibr. Spectrosc.*, **49**(2), 211–218.

Margesin, R., G. Zacke and E. Schinner. 2002. Characterization of heterotrophic microorganisms in Alpine glacier cryoconite. *Arct. Antarct. Alp. Res.*, **34**(1), 88–93.

Neu, T.R., U. Kuhlicke and J.R. Lawrence. 2002. Assessment of fluorochromes for two-proton laser scanning microscopy of biofilms. *Appl. Environ. Microbiol.*, **68**(2), 901–909.

Neu, T.R., S. Woelfl and J.R. Lawrence. 2004. Three-dimensional differentiation of photo-autotrophic biofilm constituents by multi-channel laser scanning microscopy (single-photon and two-photon excitation). *J. Microbiol. Meth.*, **56**(2), 161–172.

Neu, T.R., B. Manz, F. Volke, J.J. Dynes, A.P. Hitchcock and J.R. Lawrence. 2010. Advanced imaging techniques for assessment of structure, composition and function in biofilm systems. *FEMS Microbiol. Ecol.*, **72**(1), 1–21.

Ranjard, L. and A. Richaume. 2001. Quantitative and qualitative microscale distribution of bacteria in soil. *Res. Microbiol.*, **152**(8), 707–716.

Rippka, R., J. Deruelles, J.B. Waterbury, M. Herdman and R.Y. Stanier. 1979. Generic assignments, strain histories and properties of pure cultures of cyanobacteria. *J. Gen. Microbiol.*, **111**(2), 1–61.

Ruffell, A. and P. Wiltshire. 2004. Conjunctive use of quantitative and qualitative X-ray diffraction analysis of soils and rocks for forensic analysis. *Forensic Sci. Int.*, **145**(1), 13–23.

Schmidt, J.E. and Ahring, B.K. 1994. Extracellular polymers in granular sludge from different upflow anaerobic sludge blanket (UASB) reactors. *Appl. Microbiol. Biotechnol.*, **42**(2–3), 457–462.

Siewert, C. 2004. Rapid screening of soil properties using thermogravimetry. *Soil Sci. Soc. Am. J.*, **68**(5), 1656–1661.

Sigler, W.V. and J. Zeyer. 2002. Microbial diversity and activity along the forefields of two receding glaciers. *Microbial Ecol.*, **43**(4), 397–407.

Simon, M., H.-P. Grossart, B. Schweitzer and H. Ploug. 2002. Microbial ecology of organic aggregates in aquatic ecosystems. *Aquat. Microbial Ecol.*, **28**(2), 175–211.

Six, J., S.D. Frey, R.K. Thiet and K.M. Batten. 2006. Bacterial and fungal contributions to carbon sequestration in agroecosystems. *Soil Sci. Soc. Am. J.*, **70**(2), 555–569.

Štibal, M., M. Sabacká and K. Kaštovská. 2006. Microbial communities on glacier surfaces in Svalbard: impact of physical and chemical properties on abundance and structure of cyanobacteria and algae. *Microbial Ecol.*, **52**(4), 644–654.

Štibal, M., M. Tranter, L.G. Benning and J. Rehák. 2008. Microbial primary production on an Arctic glacier is insignificant in comparison with allochthonous organic carbon input. *Environ. Microbiol.*, **10**(8), 2172–2178.

Takeuchi, N., S. Kohshima, Y. Yoshimura, K. Seko and K. Fujita. 2000. Characteristics of cryoconite holes on a Himalayan glacier, Yala Glacier central Nepal. *Bull. Glaciol. Res.*, **17**, 51–59.

Takeuchi, N., S. Kohshima, K. Goto-Azuma and R.M. Koerner. 2001a. Biological characteristics of dark colored material (cryoconite) on Canadian Arctic glaciers (Devon and Penny ice caps). *Mem. Natl Inst. Polar Res.*, Special Issue 54, 495–505.

Takeuchi, N., S. Kohshima and K. Seko. 2001b. Structure, formation, and darkening process of albedo-reducing material (cryoconite) on a Himalayan glacier: a granular algal mat growing on the glacier. *Arct. Antarct. Alp. Res.*, **33**(2), 115–122.

Tsuneda, S., J. Jung, H. Hayashi, H. Aikawa and H. Sasaki. 2003. Influence of extracellular polymers on electrokinetic properties of heterotrophic bacterial cells examined by soft particle electrophoresis theory. *Colloids Surf. B*, **29**(2–3), 181–188.

Von Drygalski, E. 1897. Die Kryoconitlöcher. *In* Von Drygalski, E., ed. *Grønland-Expedition der Gesellschaft für Erdkunde zu Berlin 1891–1893, Vol. 1.* Berlin, W.H. Kühl, 93–103.

Wharton, R.A., Jr, C.P. McKay, G.M. Simmons, Jr and B.C. Parker. 1985. Cryoconite holes on glaciers. *BioScience*, **35**(8), 499–503.

Yee, N., L.G. Benning, V.R. Phoenix and F.G. Ferris. 2004. Characterization of metal–cyanobacteria sorption reactions: a combined macroscopic and infrared spectroscopic investigation. *Environ. Sci. Technol.*, **38**(3), 775–782.

Yoshimura, Y., S. Kohshima and S. Ohtani. 1997. A community of snow algae on a Himalayan glacier: change of algal biomass and community structure with altitude. *Arct. Alp. Res.*, **29**(1), 126–137.

Zavarzin, G.A. and T.V. Alekseeva. 2009. A puddle: an ombrophilic cyano-bacterial community. *Microbiology*, **78**(4), 468–473.

Zulpa de Caire, G., M. Storni de Cano, M.C. Zaccaro de Mulé, R.M. Palma and K. Colombo. 1997. Exopolysaccharide of *Nostoc muscorum* (Cyanobacteria) in the aggregation of soil particles. *J. Appl. Phycol.*, **9**(3), 249–253.